Int. J. Electrochem. Sci., 16 **(2021)** Article Number: 211231, doi: 10.20964/2021.12.16

International Journal of
ELECTROCHEMICAL
SCIENCE
www.electrochemsci.org

Short Communication

Influence of aging time on the corrosion behavior of 6061-T6 aluminum alloy in NaCl solution

Jinlin Yang[1], *Baozhu Zhao*[1,*], *Min Zhu*[1,*], *Li Liu*[2], *Xiang Zhang*[3]

[1] School of Mechanical Engineering & Automation, Zhejiang Sci-Tech University, Hangzhou 310018, PR China
[2] Interplex Electronic (HZ) Co., Ltd, Hangzhou 310018, China
[3] Zhejiang Zheneng Natural Gas Operation Co. Ltd., Hangzhou, Zhejiang; 310052, China
[*]E-mail: zmii666@126.com, 283396849@qq.com

Received: 18 August 2021 / *Accepted:* 27 September 2021 / *Published:* 10 November 2021

In this work, the study on the influence of aging time on the microstructure and corrosion behavior of 6061-T6 aluminum alloy in NaCl solution was systematically investigated using a series of testing methods. In the corrosion process, the two identified precipitates play different roles in the micro-galvanic corrosion cell formed with the matrix. Among them, the precipitate β serves as the anode to protect the matrix, whereas the precipitate Q causes an opposite corrosive effect. The anti-corrosion resistance of the alloy first increases and then decreases as the aging time increases. The low number of Q phase precipitates distributed within the microstructures can improve the anti-corrosion property of samples aged for 6 and 8 h. The change trend in the anti-corrosion property of alloy samples aged for different times is mainly dependent on the content of precipitate β. Therefore, the alloy sample aged for 6h possesses the best corrosion resistance because it has the highest content of precipitate β and low content of Q phase.

Keywords: Aging time; corrosion behavior; microstructure; 6061 aluminum alloy

1. INTRODUCTION

The advantages of 6061 aluminum alloy, such as low cost, medium strength, and good welding performance make it suitable for the wide application in the transportation and construction regions [1-6]. In recent years, the research on 6061 aluminum alloy has gradually increased. Panwar [7] studied aluminum 6061 red-mud composite, and the results showed that heat treatment improved the surface properties of the materials, including a reduction in the number of surface cracks. Parida [8] proposed the effect of cutting speed and nose radius in 6061 aluminum alloy machining process, and pointed out

that the force decreased as the cutting speed increased, whereas the force increased with the increase of nose radius. Fahimpour [9] found that the aging treatment improved the strength of welded 6061 aluminum alloy, but reduced its ductility. However, few studies have investigated the corrosion resistance of T6-tempered 6061 aluminum alloy. Torbati-Sarraf [10] asserted that appropriate heat-treatment could improve the corrosion resistance of the additively manufactured Al alloy. Kamal [11] indicated that different heat treatment parameters had an effect on the anti-corrosion resistance of 6061 aluminum alloy. They found that the samples without aging treatment were susceptible to intergranular corrosion, whereas over-aged samples mainly exhibited pitting corrosion. In addition, Sarah [12] reported that temperature and pH had a strong impact on the corrosion of aluminum. However, under certain circumstances, the artificially aged 6061-T6 aluminum alloy exhibited poor corrosion resistance and hardness; thus, it did not sufficiently satisfy the service requirements. Our previous research [13] indicated that the solid solution temperature could remarkably affect the microstructure and corrosion behavior of 6061-T6 aluminum alloy in NaCl solution, and found that the anti-corrosion resistance of the alloy exhibited a U-shaped trend as the solution temperature increased, and the alloy treated at 535°C had the optimal anti-corrosion property. Nevertheless, in actual applications, the aging state is always used as the service state of aluminum alloy. Therefore, based on the previous results of solution treatment research, an aging treatment was adopted to further explore the corrosion resistance of 6061-T6 aluminum alloy.

This study investigated on the most recent findings obtained by the influence of aging time on the corrosion behavior of 6061-T6 aluminum alloy in NaCl solution using electrochemical measurements and immersion test.

2. EXPERIMENTAL

2.1 Specimen and solution

The work was performed on a 5 mm thick flat plate of Al-6061-T6. The chemical composition of the plate was listed in Table 1. The plate was machined into samples with a dimension of 10 mm × 10 mm, and the sample surface was polished with a sequence of sandpapers, subsequently degreased, rinsed and dried. To investigate the influence of aging treatment on the microstructure and corrosion behavior of 6061, the samples were carried out the following heat treatment. First, the samples were subjected to solution heat treatment for 3 h at 535℃, quenched in water, and then immediately subjected to aging treatment. Subsequently, the samples were respectively held at 180°C for 1, 3, 6, and 8 h, followed by air cooling to room temperature. Subsequently, the aluminum alloy samples aged for different times were mechanically connected to copper wire and packaged with epoxy resin, leaving an exposed area of 1 cm^2 as the working surface. Then, the samples were grinded from 180 to 2000 grit emery paper, rinsed with ethanol and deionized water, and finally air-dried. A metallographic etching solution was used in accordance with GB/T 3246.1-2000. The microstructure of different aged samples was observed by scanning electron microscopy (SEM) (Quanta 250, FEI, Hillsboro, OR, USA), and the composition of precipitates was measured by energy dispersive spectroscopy (EDS).

The proportion of precipitated phases was calculated by Image-Pro Plus 6.0. In this paper, 3.5% NaCl solution with a pH of 6.7 was adopted to simulate the service environment. All tests were conducted at a fixed temperature of 25°C in a thermostatic bath.

Table 1 The composition of 6061-T6 Alloy (wt.%)

Element	Mg	Si	Cu	Fe	Cr	Mn	Zn	Ti	Al
wt.%	0.874	0.586	0.223	0.175	0.104	0.048	0.018	0.021	Bal

2.2 Electrochemical tests

The tests were performed with a three-electrode cell through a PARSTAT 2273 electrochemical workstation system. The aged alloy sample was acted as the working electrode, a saturated calomel electrode (SCE) as reference electrode and a Pt plate as counter electrode. First, the open circuit potential (OCP) of the alloy sample was performed for 30 min to stabilize the system. Then, EIS curve was tested under a range of 100 kHz - 10 mHz with a disturbing signal amplitude of 10 mV. And the measurement of potentiodynamic polarization curve was performed at a scanning rate of 0.5 mV/s with a potential range of -1.2 V (vs. SCE) to -0.6 V (vs. SCE).

2.3 Immersion test

Various aged specimens were soaked in the solution for 168 h. After testing, the remaining precipitated phase was detected by EDS. Then, a chromic anhydride solution was adopted to remove the corrosion products formed on the alloy surface. Subsequently, the corrosion morphology of different aged samples was analyzed via SEM. The above measurement was repeated at least three times.

3. RESULTS

3.1 Microstructure analysis

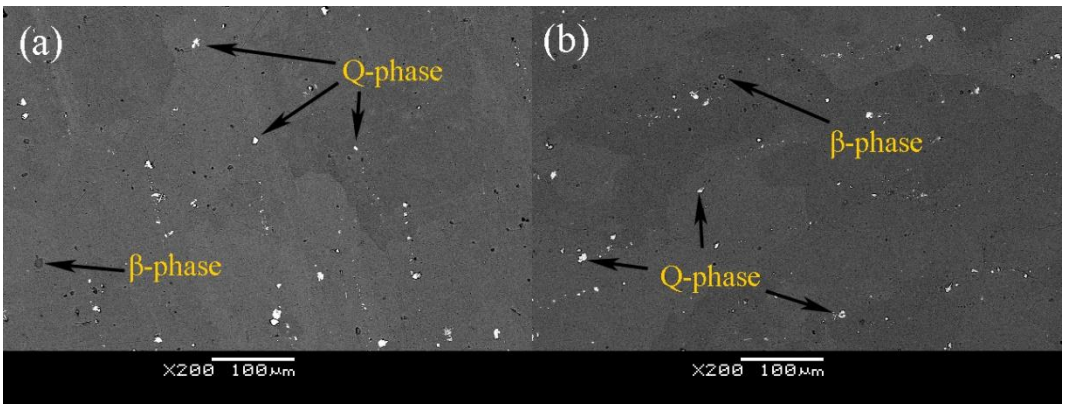

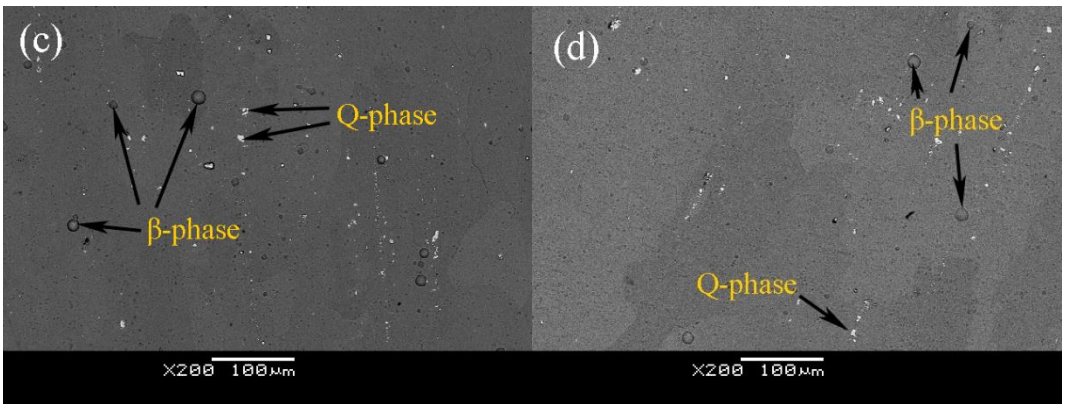

Figure 1. Microstructures of 6061 aluminum alloy samples treated at 180°C for different aging times. (a) 1 h; (b) 3 h; (c) 6 h; (d) 8 h

Figure 1 exhibits the microstructure of the alloy samples prepared at various aging times. Apparently, white and grey precipitates are dispersed in the aluminum matrix of different specimens. The two precipitates were analyzed by EDS, and the results are shown in Figure 2.

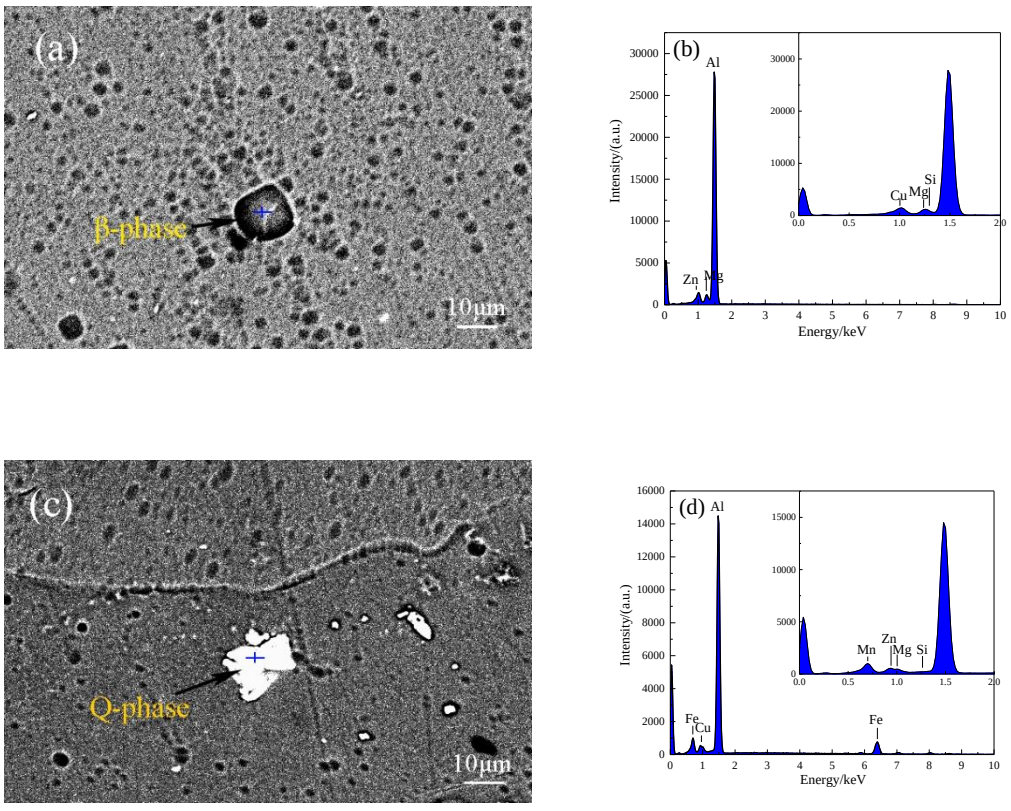

Figure 2. SEM images and element analysis of two precipitates within the aged alloy (a)(b) β-phase; (c)(d) Q-phase.

The first precipitate is light-black, and exhibits a nearly spherical shape. The EDS result in Figure 2b indicates that this precipitate-referred to hereinafter as precipitate β, mainly consists of Al,

Mg, Si, Cu and Zn. As shown in Figure 2c and 2d, the other precipitate-referred to hereinafter as precipitate Q is white, irregularly-shaped, and mainly consists of Al, Fe, Mg, Si, Cu, Zn and Mn. Different sized precipitates Q are randomly distributed in all aged samples. Obviously, when the aging time increases up to 6 h, the size of precipitate β becomes large, and its content in the sample is high. The content of precipitates on the surface of different aged samples was calculated, and the result was shown in Figure 3. Clearly, the fraction of precipitate β increases first and then decreases, and the content of precipitate β is the highest in the sample aged for 6h. And the size and content of precipitate Q reveal an decreasing trend.

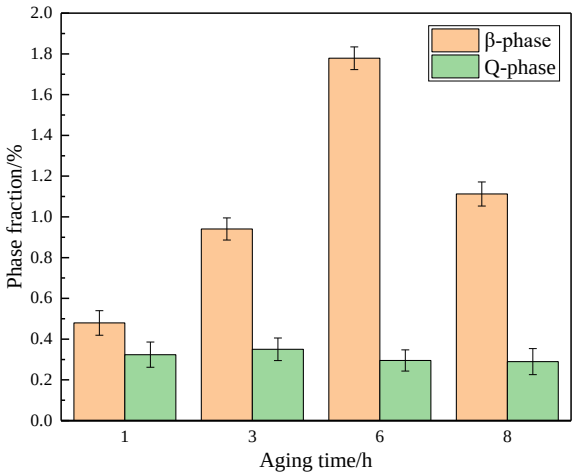

Figure 3. Percentage of two precipitates within alloy samples treated at 180°C for different aging times.

3.2 Electrochemical measurements

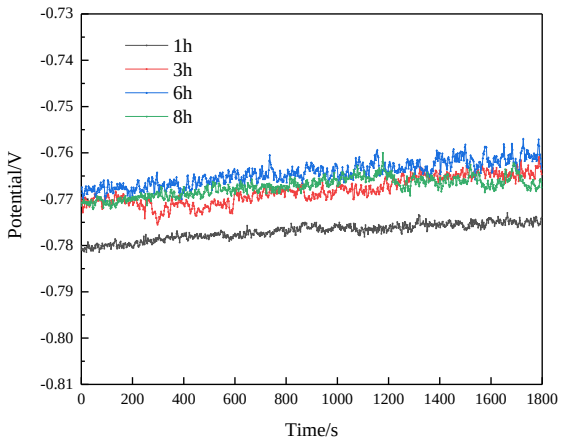

Figure 4. Corrosion potential versus time curves of alloy samples treated at 180°C for different aging times in 3.5% NaCl solution.

Figure 4 shows the OCP curves of alloy samples treated for various aging times. In all of the curves, the corrosion potential increases slightly with the increase of testing time, and finally reaches a relatively stable value. Obviously, the sample aged for 6 h has the most positive potential, indicating that the corrosion trend of the sample is the lowest. In contrast, the specimen aged for 1 h displays the most negative potential, suggesting that it possesses the highest corrosion trend.

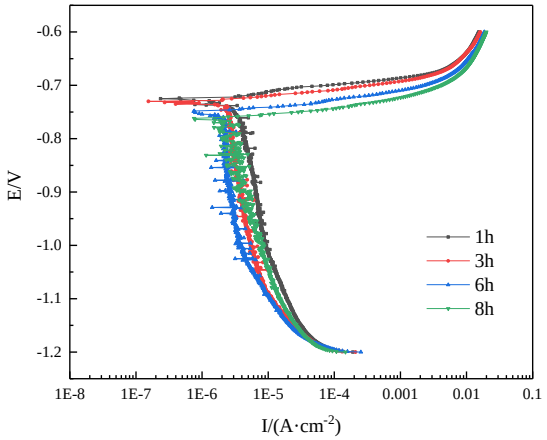

Figure 5. Potentiodynamic polarization curves of alloy samples treated at 180°C for different aging times in 3.5% NaCl solution.

Figure 5 exhibits the potentiodynamic polarization curves of various aged samples. All of the curves exhibit the similar shape. In the anode branch, a distinct active dissolution characteristic is displayed [14], whereas the oxygen diffusion reaction predominantly controls the cathode part, suggesting that various aged samples have a similar corrosion mechanism. The fitted corrosion current density (I_{corr}) of various aged samples is shown in Figure 6. As the aging time gradually increases, I_{corr} first decreases and then increases. Thus, the sample aged for 6 h has the minimum value, whereas that of the specimen aged for 1 h is the highest. This means that the former exhibits the lowest corrosion rate, and the latter has the highest corrosion rate [15-17].

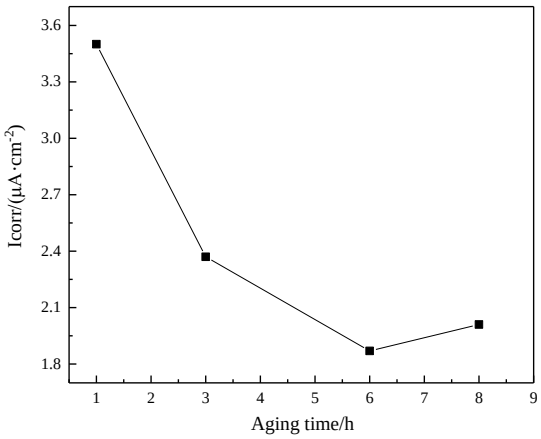

Figure 6. Icorr of specimens treated at 180°C for different aging times in 3.5% NaCl solution.

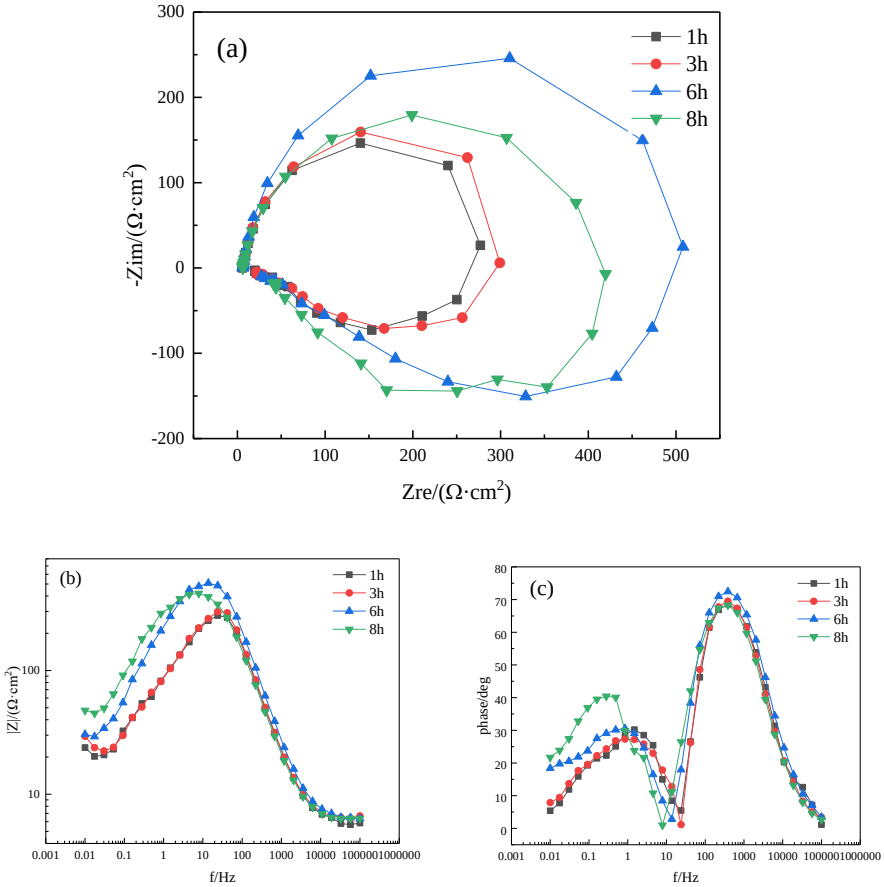

Figure 7. Impedance spectrum of alloy samples treated at 180°C for different aging times in 3.5% NaCl solution. (a) Nyquist plot; (b, c) Bode plot

Figure 7 shows the Nyquist and Bode plots of various aged samples. All curves consist of the similar semicircular capacitive and inductive reactance arcs. The presence of inductive arc may be related to the adsorption/desorption behavior of chloride ions. The diameter of semicircular-arc in Nyquist plot could be used to assess the anti-corrosion resistance of the materials [18]. The larger diameter of the semicircular-arc means that the sample has the better corrosion resistance. The characteristics of low frequency region indicate that a dispersion effect exists in the electrode response [19]. The two peaks in Figure 7c correspond to two time-constants. To further illustrate the corrosion behavior of different aged samples, an equivalent circuit was used to fit the data (Figure 8). The circuit contains five components: solution resistance (R_s), charge transfer resistance (R_t), inductive resistance (R_l), inductive element (L) and nonideal double layer capacitance (Q). As listed in Table 2, compared with other samples, the sample aged for 6 h has the largest semicircular-arc diameter and the maximum Rt value. This suggests that the sample aged for 6h has the best anti-corrosion resistance. In contrast, the sample aged for 1 h has the minimum R_t value, indicating that it exhibits the poor corrosion resistance [20-22]. It should be noted that the oxide film formed on the alloy surface was removed during the process of sample preparation.

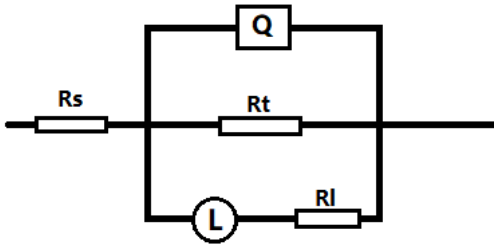

Figure 8. Equivalent circuit used for fitting EIS data.

Table 2. The fitted electrochemical parameters of different aged samples.

Aging time (h)	Rs ($\Omega \cdot cm^2$)	Q ($\times 10^{-6}\ \Omega^{-1} \cdot s^n \cdot cm^{-2}$)	n (0<n<1)	Rt ($\Omega \cdot cm^2$)	L (H)	Rl ($\Omega \cdot cm^2$)
1	6.106	9.754	0.9701	245	14.92	33.18
3	6.705	8.512	0.9862	261.8	13.21	40.85
6	6.678	7.563	0.9737	447.8	59.14	44.33
8	6.403	13.59	0.941	386.5	121.3	48.19

3.3 Immersion test

Figure 9 displays the corrosion morphologies of various aged specimens soaked in the solution for 168 hours after removing the surface corrosion products. Apparently, the corrosion degree of different aged samples is different. Figure 9a exhibits the severe corrosion characteristics. A great amount of different sized pits are distributed on the surface of the sample aged for 1 h. These pits continually dissolve and generate large sized corrosion pits. The corrosion morphology of the sample aged for 3 h is displayed in figure 9b. The corrosion status of the sample is similar to that of specimen aged for 1 h, however, the sample aged for 3 h has notably fewer large sized pits. In contrast, the sample aged for 6 h (figure 9c) shows the slightest corrosion characteristics, with only a few small pits on the substrate surface. In figure 9d, the decreasing number of corrosion pits indicates that the corrosion status of specimen aged for 8 h is slighter than those of samples treated at aging times of 1h and 3h. Thus, it can be concluded that the anti-corrosion resistance of alloy sample first increases and then decreases as the aging time increases.

Furthermore, it is clearly seen that the remaining white precipitates are embedded in the pits or distributed on the surface of various aged samples. Some pits are located around the precipitates. This feature indicates that the precipitates can affect the corrosion behavior of alloy [23-29]. The white precipitates inside the pits occurred on the corroded samples were analyzed. The results in Figure 10 indicate that the remaining precipitates are phase Q. This may be attributed to the formation of micro-galvanic corrosion cell. In the corrosion process, the precipitate Q acts as the cathode, thus it is protected. And the substrate serves as the anode, and is subjected to the corrosion dissolution[30]. Hence, the pits are generated on the substrate. As revealed in Figure 3, as aging time increases, the content of precipitate Q decreases. Therefore, the content of precipitate Q results in a different

influence on the corrosion resistance of alloy samples aged for different times. The low number of Q phase precipitates distributed within the microstructures can improve the anti-corrosion property of samples aged for 6 and 8 h.

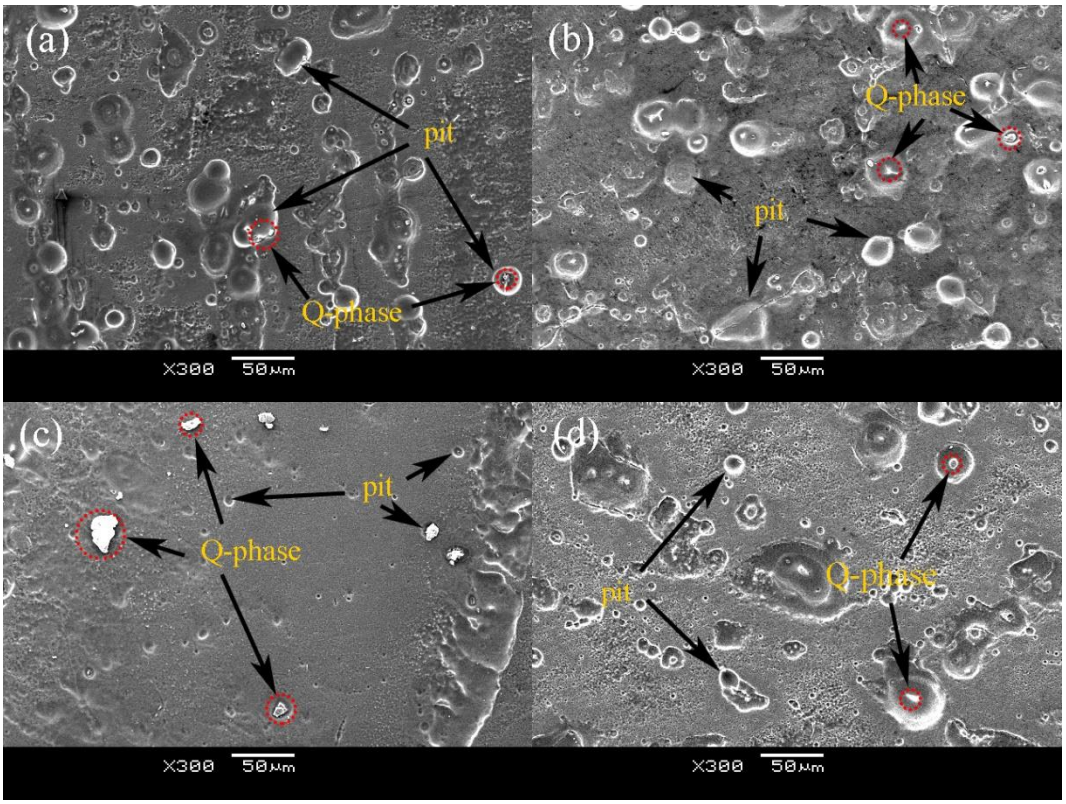

Figure 9. Corrosion morphologies of different aged samples immersed for 7d after removing the corrosion products. (a) 1h; (b) 3h; (c) 6h; (d) 8h

However, the precipitate β is not observed on the surface of the corroded samples treated for various aging times. It is reasonable to believe that the precipitate β acts as the anode phase in the micro-galvanic corrosion cell formed with the matrix. Consequently, it preferentially dissolves, thereby protecting the substrate and improving the corrosion resistance of alloy sample. Figure 3 shows a substantial difference in the content of precipitate β among the different samples. Thus, the U-shaped trend in the corrosion resistance of alloy samples is mainly dependent on the corresponding content of precipitate β. Therefore, the alloy sample aged for 6 h possesses the best corrosion resistance because it has the highest content of precipitate β and low content of Q phase.

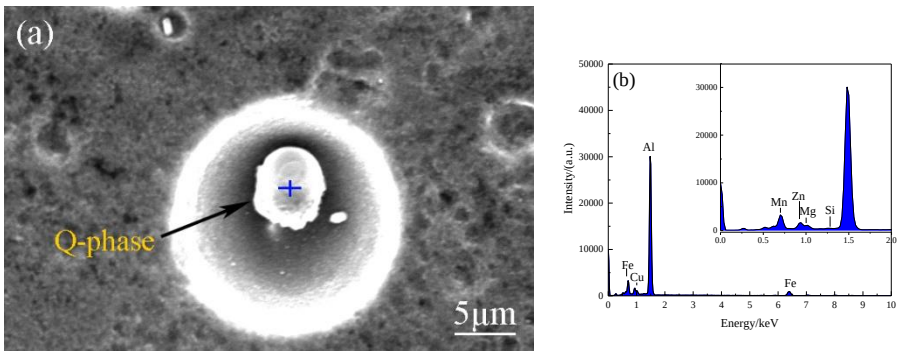

Figure 10. SEM images (a) and EDS analysis (b) of white precipitate distributed inside the pit.

4. CONCLUSIONS

In the corrosion process, the two identified precipitates-denoted precipitate β (Al, Mg, Si, Cu and Zn) and precipitate Q (Al, Fe, Mg, Si, Cu, Zn and Mn) play different roles in the micro-galvanic corrosion cell formed with the matrix. Among them, the precipitate β serves as the anode phase to protect the substrate, whereas the precipitate Q generates an opposite corrosive effect. The corrosion resistance of alloy samples first increases and then decreases as the aging time increases. The low amount of Q phase precipitates distributed within the microstructures can improve the anti-corrosion property of samples aged for 6 and 8 h. The change trend in the anti-corrosion resistance of alloy samples treated for different aging times is mainly dependent on the corresponding content of precipitate β. Therefore, the alloy sample aged for 6 h exhibits the best corrosion resistance because it has the highest content of precipitate β and low content of Q phase.

ACKNOWLEDGEMENTS
This work was supported by the Natural Science Foundation of Zhejiang Province of China (No. LY18E010004) and National Material Environmental Corrosion Infrastructure.

References

1. V.M. Khojastehnezhad and H.H. Pourasl, *T. Nonferr. Metal. Soc. China*, 28(2018)415.
2. K.N. Salloomi, *J.Manuf.Process*, 45(2019)746.
3. S. Sivananthan, K. Ravi and C. Samson Jerold Samuel, *Mater. Today: Proceedings,* 21(2020)968.
4. C.Y. Cui, T.Y. Wan, Y.X. Shu, S. Meng, X.G. Cui, J.Z. Lu and Y.F. Lu, *J. Alloy. Compd.*, 803(2019)1112.
5. J. Yi, G. Wang, S.K. Li, Z.W. Liu and Y.L. Gong, *T. Nonferr. Metal. Soc*., 29(2019)2035.
6. S.S. Razavi-Tousi, R. Yazdani-Rad and S.A. Manafi, *Mater. Sci. Eng. A*, 528(2011)1105.
7. N. Panwara, A. Chauhanb, H.S. Palia and M.D. Sharmaa, *Mater. Today: Proceedings,* 21(2020)2014.
8. A.K. Parida, P.V. Rao and S. Ghosh, *Mater. Today: Proceedings,* 27(2020)2569.
9. V. Fahimpour, S.K. Sadrnezhaad and F. Karimzadeh, *Metall Mater. Trans. A*, 44(2013)2187.
10. H. Torbati-Sarraf, S.A. Torbati-Sarraf, N. Chawla and A. Poursae, *Corros.Sci.,* 174(2020)No.108838.

11. E.M. Kamal, A. El-Sayed, E. Mohammed, A. Hafez and M. Saed, *Corros.Sci.,* 54(2012)167.
12. L. Sarah, M. Laot, K. Colas, B. Kapusta, S. Delpech and D. Gosset, *J. Alloys Compd.,* 833(2020)No.155146.
13. M. Zhu, B.Z. Zhao, Y.F. Yuan, S.Y. Guo and J. Pan, *J. Mater. Eng. Perform*., 29(2020)4725.
14. M. Zhu, Y. F. Yuan, S. M. Yin, G. H. Yu, S. Y. Guo, Y. Z. Huang and C. W. Du, *J. Mater. Eng. Perform*., 28(2019)1698.
15. X.L. Zhang, Z.H. Jiang, Z.P. Yao, Y. Song and Z.D. Wu, *Corros. Sci.,* 51(2009)581.
16. M. Curioni, *Electrochim. Acta*, 120(2014)284.
17. D.I. Tishkevich, A.I. Vorobjova, D.L. Shimanovich, D.A. Vinnik, T.I. Zubar, A.L. Kozlovskiy, M.V. Zdorovets, D.V. Yakimchuk, S.V. Trukhanov and A.V. Trukhanov, *J. Alloy. Compd.*, 804(2019)139.
18. C.N. Cao, *Electrochim. Acta*, 35(1990)831.
19. L.H. Yang, Y.X. Wan, Z.L. Qin, Q.J. Xu and Y.L. Min, *Corros. Sci.*, 130(2018)85.
20. M. Liu, X.Q. Cheng, X.G. Li and T.J. Lu, *J. Electroanal. Chem.*, 803(2017)40.
21. M. Liu, X.Q. Cheng, X.G. Li, Y. Pan and J. Li, *Appl. Surf. Sci.*, 389(2016)1182.
22. M. Liu, X.Q. Cheng, X.G. Li, C. Zhou and H.L. Tan, *Constr. Build. Mater.*, 130(2017)193.
23. J.A. Lyndon, R.K. Gupta, M.A. Gibson and N. Birbilis, *Corros. Sci.*, 70(2013)290.
24. S. Jain, M.L.C. Lim, J.L. Hudson and J.R. Scully, *Corros. Sci*., 59(2012)136.
25. V.A. Katkar, G. Gunasekaran, A.G. Rao and P.M. Koli, *Corros. Sci*., 53(2011)2700.
26. J. Datta, B. Samanta, A. Jana, S. Sinha, C. Bhattacharya and S. Bandyopadhyay, *Corros. Sci*., 50(2008)2658.
27. T.J. Watson, M.A. Gordillo, A.T. Ernst, B.A. Bedard and M. Aindow, *Corros. Sci.*, 121(2017)133.
28. I. Guzmán, E. Granda, J. Acevedo, A. Martínez, Y. Dávila and R. Velázquez, *Materials*, 12(2019)No.4157.
29. L.L. Ren, H.M. Gu, W. Wang, S. Wang, C.D. Li, Z.B. Wang, Y.C. Zhai and P.H. Ma, *Materials*, 12(2019) No.4160.
30. R. Ambat and A.J. Davenport, *Corros. Sci.*, 48(2006)3455.